Schottky Mass Measurements of Stored and Cooled Neutron-Deficient Projectile Fragments in the Element Range of $57 \leq Z \leq 84$

October 27, 1999

T. Radon[a,1], H. Geissel[a,e], G Münzenberg[a,g], B. Franzke[a], Th. Kerscher[b], F. Nolden[a], Yu. N. Novikov[c], Z. Patyk[f], C. Scheidenberger[a], F. Attallah[a], K. Beckert[a], T. Beha[b], F. Bosch[a], H. Eickhoff[a], M. Falch[2], Y. Fujita[d], M. Hausmann[a,e], F. Herfurth[a], H. Irnich[a], H. C. Jung[e], O. Klepper[a], C. Kozhuharov[a], Yu. A. Litvinov[c], K. E. G. Löbner[b], F. Nickel[a], H. Reich[a], W. Schwab[a], B. Schlitt[a], M. Steck[a], K. Sümmerer[a], T. Winkler[a], H. Wollnik[e]

[a] *Gesellschaft für Schwerionenforschung, Planckstrasse 1, D-64291 Darmstadt, Germany*
[b] *Sektion Physik, Ludwig-Maximilians-Universität München, Am Coulombwall 1, D-85748 Garching, Germany*
[c] *St. Petersburg Nuclear Physics Institute, Gatchina 188350, Russia*
[d] *College of General Education, Osaka University, Osaka 560, Japan*
[e] *II. Physikalisches Institut, Universität Giessen, Heinrich-Buff-Ring 16, D-35392 Giessen, Germany*
[f] *Soltan Institute for Nuclear Studies, Warsaw, Poland*
[g] *Johannes Gutenberg-Universität Mainz, Germany*

Abstract

A novel method for direct, high precision mass measurements of relativistic exotic nuclei has been successfully applied in the storage ring ESR at GSI. The nuclei of interest were produced by projectile fragmentation of 930 MeV/u bismuth ions, separated in-flight by the fragment separator FRS, stored and cooled in the ESR. The mass values have been deduced from the revolution frequencies of the coasting cooled ions. We have measured 115 new mass values with a precision of about 100 keV and a resolving power of $3.5 \cdot 10^5$ for the neutron-deficient isotopes of the elements $57 \leq Z \leq 84$. This paper presents the experimental method, the mass evaluation and a table of the experimental mass values.

PACS number 21.10.Dr, 27.70.+q, 27.80.+w, 29.20.Dh, 29.30.Aj

[1]Corresponding author. Tel.: +49-6159-71-2142; fax: +49-6159-71-2902; e-mail: T.Radon@gsi.de.

1 Introduction

The mass of a nucleus is a basic property which reflects the total binding energy of the nucleons. It determines the stability of the nucleus and gives information about its structure. Systematic studies of nuclear masses as a function of neutron number N and proton number Z have revealed important properties such as shell closures and changes of the nuclear shape.

Present nuclear models are based on effective nuclear forces developed from the properties of nuclei at or close to the valley of beta stability. Basic features of nuclei far off stability, such as large neutron or proton excess, are often not included [1, 2, 3]. As a consequence theories cannot properly handle the isospin and density dependence. Therefore, masses far off stability are sensitive probes for nuclear models [4] and necessary for their further development. Of special interest are the most exotic species located near the drip lines, at closed shells far off stability or along the paths of cosmic nucleosynthesis. The present situation of known and unknown masses is shown in Fig. 1 where those nuclei are presented which exist as bound systems according to Ref. [8] Our experimental knowledge of the mass surface is based on various direct

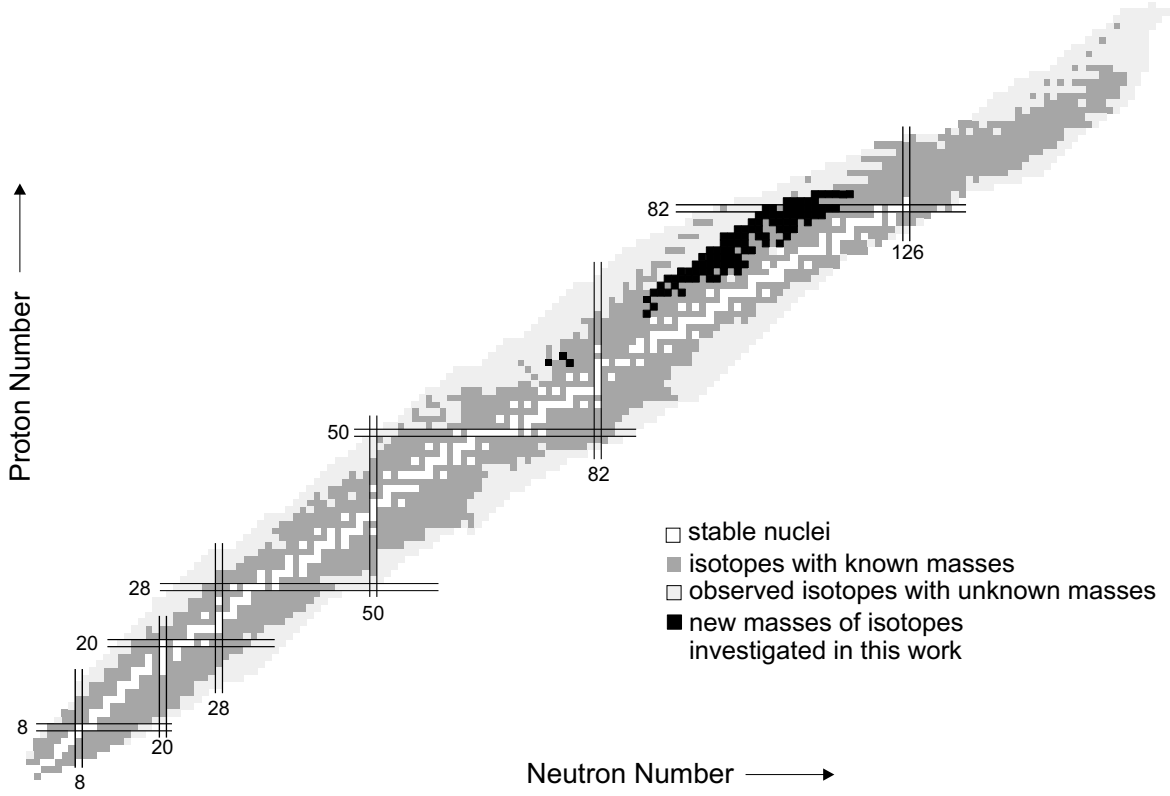

Figure 1: Known masses and unknown masses according to ref. [7] are indicated. The region of nuclei with previously unknown masses that were determined in the present experiment is marked with a black area.

and indirect methods combined with a careful evaluation and adjustment of the set of the experimental data [5, 6, 7, 8]. Figure 1 shows 1840 nuclides with measured masses and about 1100 known nuclides far from stability which have been observed but whose masses are not known yet. A recent review [11] summarizes the experimental and

theoretical progress in the field. The pioneering experiments for mass determination of exotic nuclei used electro-magnetic spectrometers [12]. The precision of these conventional spectrometers is limited by the ion-optical resolving power combined with the intensity requirement for exotic nuclei. Direct mass measurements of light nuclides far off stability have been performed with the high resolution spectrometers SPEG [9] and TOFI [10] employing projectile fragmentation and target spallation, respectively. Recently, methods based on frequency measurements have been developed, see [11, 13, 14, 15] and references therein which are superior in accuracy and resolution compared to electro-magnetic spectrometers. The highest precision in mass measurements is presently achieved with Penning traps where low-energy ions are stored and cooled [13, 14]. The combination of a trap system with a radioactive nuclear beam facility is realized with the ISOLTRAP at CERN [16]. Masses of exotic nuclei have been determined with an accuracy of 10^{-7}.

In this paper we present a new experimental method for direct mass measurement [17]. Projectile fragments with relativistic energies are separated in-flight and injected into a storage ring. Electron cooling reduces the relative velocity spread of the fragments to values of smaller than 10^{-6} such that their revolution frequency is primarily determined by the ionic mass-to-charge ratio. The revolution frequencies are obtained from the Fourier transform of the Schottky noise signal of the coasting beam [18].

The method presented here has several unique features and clear advantages. A storage ring is a modern experimental facility of large acceptance. Consequently fragment beams can be injected with a high efficiency which permits mass measurements of very exotic species. A large number of different isotopes can be stored simultaneously. This is not only an advantage for calibration with known reference masses but also facilitates to investigate large areas of the nuclear chart in a systematic way. Each isotope has been stored in various ionic charge states which provide redundant measurements and allows to establish a consistent network of masses. To fully profit from the many-fold correlations, a method was developed to convert the measured frequencies to masses in a network with consistent errors. The experiment was carried out at the GSI secondary beam facility which offers unique possibilities for the production and study of exotic nuclei over the entire range of the chemical elements up to the uranium region. The heavy-ion synchrotron SIS can provide beams of all stable nuclides from protons up to uranium with maximum kinetic energies corresponding to a magnetic rigidity of $B\rho = 18$ Tm [19]. The beams of relativistic exotic nuclei are produced in a reaction target by fragmentation or fission of the projectiles in peripheral nuclear collisions. In-flight separation of the projectile fragments with the fragment separator FRS provides nuclei with half-lives down to the sub–μs range independent of the chemical properties of the produced elements [20]. Due to the spatial separation in flight, the secondary beams can be injected into beam-lines and transported to dedicated experimental areas, including the experimental storage ring ESR [21], for nuclear reaction and structure studies. A specific advantage of in-flight projectile separation is the option, besides the spatial separation of mono-isotopic beams, to select beams with the same $B\rho$, covering a set of nuclides from a well defined area of the chart of nuclides [20]. We performed already several pilot experiments at FRS-ESR in the light mass region [22, 23] and one with fragmentation of gold [24]. Here we present a large-scale mass measurement for neutron-deficient nuclei in the lead region using a ^{209}Bi projectile fragmentation. Only very few masses were known in this mass

region as shown in Fig. 1. Moreover, it includes an extended area of α-emitters with unknown masses [25, 26]. A mass measurement of one of the nuclei at the end of an α-decay chain allows one to determine the masses of all nuclides along the linked α-chains. The results including the complete α-chain information will be presented in a forthcoming paper.

2 Experimental method

2.1 Production and separation of relativistic projectile fragments

In the present experiment (see Fig. 2)the SIS has provided a beam of $^{209}Bi^{67+}$ ions with an energy of 930 MeV/u. Up to $5{\cdot}10^7$ ions were extracted with fast extraction. The beam was focused on an 8 g/cm^2 beryllium target placed at the entrance of the FRS. The primary beam and the projectile fragments emerge from the production

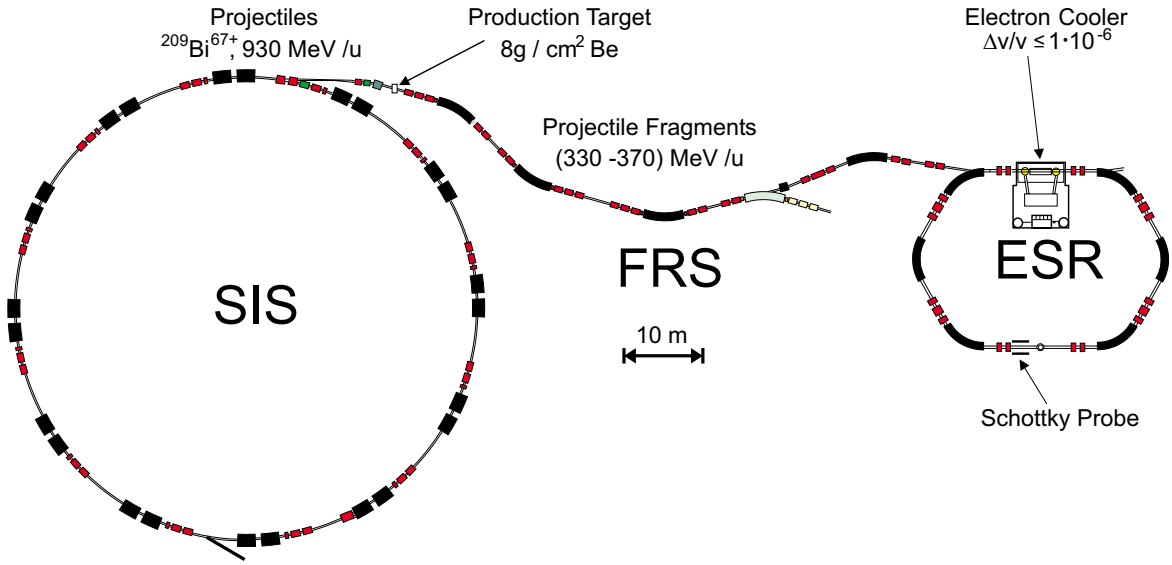

Figure 2: Layout of the high-energy facilities at GSI used for mass measurements of exotic nuclei.

target with kinetic energies of about 330–370 MeV/u. At these energies the beam and the fragments carry only few electrons or are fully stripped behind the target. In our experiment the magnetic fields of the FRS and the ESR were both set to various magnetic rigidities. The ionic charge state population of fragments emerging from the beryllium target is shown in Fig. 3 for a representative magnetic rigidity of 6.7 Tm. The abundance has been calculated with a model based on measurements at GSI and LBL [27]. Bare, H-like, and He-like ions were mainly measured in our experiment.

In principle, projectile fragmentation leads to all nuclei which can be generated by the removal of nucleons from the projectile, i.e., they can range from isotopes of the element of the projectile down to protons. However, the production cross-sections strongly decrease with the increasing number of removed nucleons. Reliable estimates of fragmentation cross-sections can be obtained from the semi-empirical parametrization implemented in the EPAX code [28]. The prediction for the formation cross

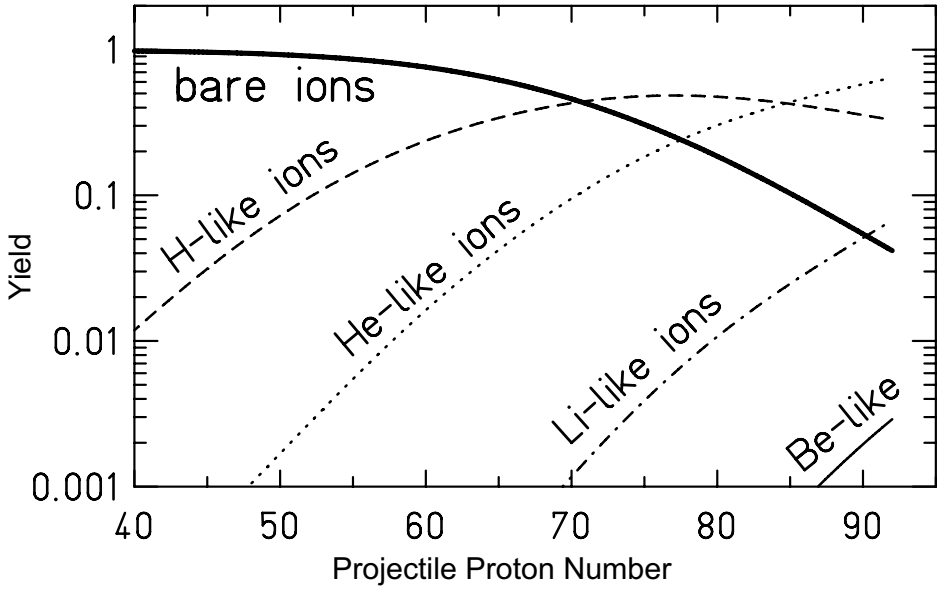

Figure 3: Calculated ionic charge state population of heavy ions [27] emerging from a beryllium target with velocities corresponding to a fixed magnetic rigidity of 6.7 Tm. Masses of stable nuclei were used in these calculations.

sections of ^{209}Bi fragments in a beryllium target are presented as contour lines in the chart of nuclei, see Fig. 4. Furthermore, by nuclear charge-exchange reactions, also isotopes of the element above the projectile, here polonium nuclei, are abundantly produced.

2.2 Injection, storage, and cooling of projectile fragments in the ESR

In the present experiment, the FRS was used without an energy degrader in the dispersive mid focal plane. Thus all ions with the same magnetic rigidity were transmitted. The preparation and analysis of the experiment has been guided by computer simulations since the complex conditions including the ion-optical transmissions cannot be accurately estimated with pure analytical methods. For the calculation of the fragment distributions created in the production target and transmitted through the ion-optical systems the Monte-Carlo code MOCADI [29] is used. In the programme the cross sections characterizing the nuclear and atomic processes of the projectile–target interaction, the corresponding reaction kinematics, the atomic slowing down in matter, and the ion-optical properties of FRS and ESR are implemented. In Fig. 5 the important steps from the fragmentation process to the observed Schottky frequency-spectrum are presented as a result of such Monte-Carlo simulations. In the selected example the goal was to inject and to measure bare ^{197}Bi nuclei and all masses within the same $B\rho$-window. To facilitate the understanding of the present example only bare bismuth isotopes are plotted with an assumed mean $B\rho$ value of 6.7 Tm. The kinetic energy of the primary beam amounts to 930 MeV/u before the target and 350 MeV/u after the penetration of the target. The length of the bar for each Bi isotope corresponds to the FWHM of the velocity distribution. The $B\rho$ windows of ± 1 % for the transmission through the FRS and of ± 0.35 % for the injection acceptance of the ESR kicker

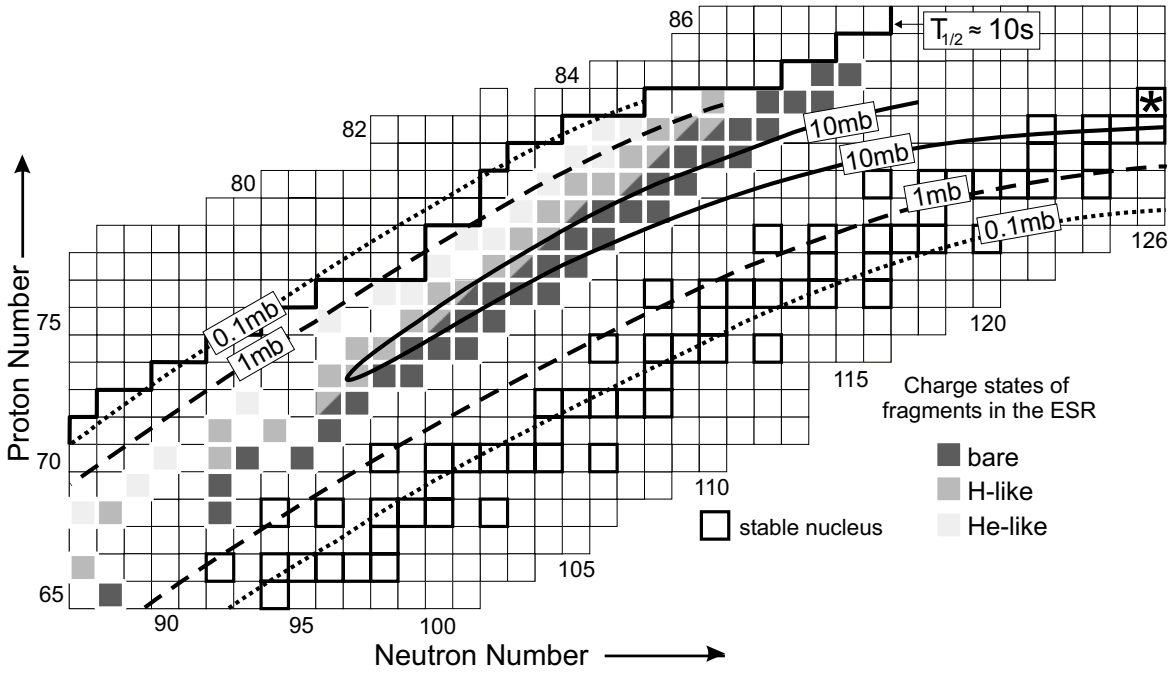

Figure 4: Production cross-sections [28] predicted for projectile fragmentation of ^{209}Bi projectiles in beryllium. The charge states of the fragments are indicated as recorded in the Schottky spectra at a $B\rho$ setting of 6.7 Tm. The helium-like ions approach the 10s-line, which at this time was a half-life limitation in our experiment.

magnet are indicated by full and dashed vertical lines respectively. Both areas are centered at the selected mean $B\rho$ value. Assuming that the kicker acceptance represents the limitation of the accepted phase space the enclosed isotopes can be stored in the ESR and cooled by merging an electron beam. The injected fragments are characterized by velocity distributions with widths of $\delta v/v \simeq 4 \cdot 10^{-3}$ (full lines). By electron cooling all ions are forced to the same mean velocity β_{cooler}. The resulting width of the distributions is $\delta v/v \simeq 7 \cdot 10^{-7}$. Due to the cooling, the fragments fully occupy the $B\rho$ acceptance of the ESR. The full circles denote species, which fall within the acceptance of the ESR, while the open dots denote ions whose magnetic rigidity after cooling is outside of the ESR storage acceptance. In reality the experimental conditions are more complex than illustrated in Fig. 5, i.e., we have a broad distribution of elements where the isotopes populate different ionic charge states, see Figure 3, and have wide velocity distributions depending on the A and Z difference to the primary beam. For optimum cooling condition the number of stored ions and the velocity of the cooler electron have to be carefully selected. The cooling process contracts the phase space of the injected beams until a balance is reached between the cooling force and the intra-beam scattering due to Coulomb interaction between the stored ions. The equilibrium momentum spread depends critically on the number n of stored ions. At intensities with $n \geq 10^4$ ions, the relative momentum spread of the cooled beams increases as $\delta p/p \propto n^{1/3}$. However, for low-intensity beams with particle numbers $n \lesssim 5 \cdot 10^3$, a suppression of the intra-beam scattering is observed [18], and thus a velocity spread as small as $\delta p/p \lesssim 7 \cdot 10^{-7}$ is achieved by the cooling. This condition improves the mass resolving power and therefore the intensity must be kept quite low.

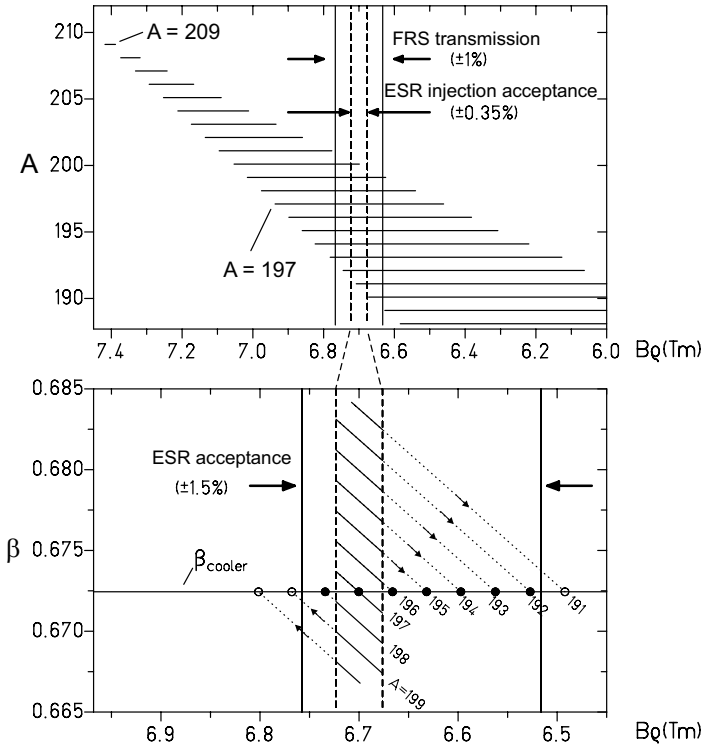

Figure 5: Scheme of production, separation and cooling of bare bismuth fragments illustrated in the $B\rho$ space. Upper part: Calculated magnetic-rigidity distributions of bismuth isotopes at the exit of the 8 g/cm^2 beryllium target. Lower part: Velocity spread (in units of the velocity of light $\beta = v/c$) as a function of the magnetic rigidity of the stored and cooled bismuth fragments. The injected fragments are characterized by incident velocity distributions with widths of $\delta v/v \simeq 4 \cdot 10^{-3}$ (slanting full lines).

The cooling time is roughly proportional to the third power of the velocity difference between the electron beam and the fragments to be cooled. With electron densities of typically $3{\cdot}10^6$/cm^3 , corresponding to a cooler current of about 200 mA along a 2 m straight section, most of the "hot" fragment beams can be cooled in about 30 s. In order to measure fragments with shorter half-lives, the velocity of the cooler electrons was chosen to be close to the mean velocity of the injected fragments. By this method nuclei with half-lives of $T_{1/2}$ $\geq$12 s have been cooled and could be observed in the frequency spectra.

2.3 Schottky mass spectrometry

Schottky noise spectroscopy [30] is widely used for non-destructive beam diagnosis in circular accelerators and storage rings. Signals induced by the stored circulating ions in probes are recorded and analyzed. Already in our pilot experiments with cooled projectile fragments [22, 23] we have applied Schottky diagnostics. Since then, we have gradually improved this technique for the requirements of precise mass spectrometry [24, 25, 26, 31, 32, 33].
At each turn, the stored ions, circulating in the ESR with revolution frequencies of about 2 MHz, induce a mirror charge on electrostatic pick-up electrodes installed in the ring. Each species of the circulating multi-component ion beam has its own mean

revolution-frequency with $f_i = v_i/C_i$, v_i and C_i being its velocity and length of its closed orbit, respectively. A typical mean storage orbit in the ESR is $C = 108.4$ m. As C_i depends on the mass-to-charge ratio $(m/q)_i$, we obtain to first order for two resolved peaks i, j in the revolution frequency spectrum for the relative frequency difference:

$$\frac{f_i - f_j}{f_i} = -\alpha_p \cdot \frac{(m/q)_i - (m/q)_j}{(m/q)_i} \tag{1}$$

where $\alpha_p = dC/C/(d(B\rho)/(B\rho))$ is the momentum compaction factor. This ion-optical parameter characterizing the relative variation of the orbital length C per relative variation of the magnetic rigidity $B\rho$ has a value of approximately 0.14 in our experiment. The width of a frequency distribution is determined by the width of the momentum and velocity distribution of a selected fragment:

$$\frac{\delta f_i}{f_i} = \left(\frac{1}{\gamma_i^2} - \alpha_p\right) \cdot \frac{\delta p_i}{p_i} = \left(\frac{1}{{\gamma_i}^2} - \alpha_p\right) \cdot {\gamma_i}^2 \cdot \frac{\delta v_i}{v_i} \tag{2}$$

where γ_i represents the relativistic Lorentz factor, and $\delta p_i/p_i$ and $\delta v_i/v_i$ are the relative widths of the momentum and velocity distributions for a selected fragment, respectively. When the ions are cooled they are forced to the same mean velocity with a small velocity spread thus their frequency distributions become very narrow and a high mass resolving power can be achieved.

The two equations are the basis for the Schottky Mass Spectrometry (SMS). If α_p and the mass-to-charge ratio of a reference ion are precisely known, unknown masses can be determined by application of Eq. (1). Generally also α_p is obtained by means of Eq. (1) using the lines of ions with well known m/q values. The mean values of the frequency distributions $f_{i,j}$ represent the main observables of SMS. The mass resolving power R_m is given by:

$$R_m = \left| -\alpha_p \cdot \frac{f}{\delta f} \right| = \left(\frac{\alpha_p}{1 - \gamma^2 \alpha_p}\right) \cdot \frac{v}{\delta v} \tag{3}$$

for $1/\gamma^2 > \alpha_p$ This equation shows that the reduction of the velocity spread $\delta v/v$ is crucial for achieving a high mass-resolving-power. For example, the mass resolving power for a 350 MeV/u uncooled fragment beam would be only about 50, however, we achieved with cooled beams in the present experiment a mass resolving power of 350000.

In the experiment, due to technical reasons the Schottky noise signal of the 16^{th} harmonic of the revolution frequency was analyzed. After amplification and down-mixing by a suitable rf-frequency of typically 30 MHz provided by a local oscillator, small frequency bands of 10 kHz or 100 kHz were selected depending on the needed frequency resolution. The bandwidth of 100 kHz covers a large part of the orbits allowed by the ESR $B\rho$-acceptance. These low-frequency bands were sampled for 160 ms and 16 ms, respectively, and Fourier analyzed by real-time fast Fourier transformation (FFT) with 1601 frequency channels. Subsequently up to 10^4 samples were averaged in order to achieve a high signal-to-noise ratio. A low-resolution 100-kHz spectrum is shown in the upper part of Fig. 6. In this example, the magnetic rigidity of the FRS and of the ESR and the voltage of the electron cooler (U = 181 kV) and its electron current

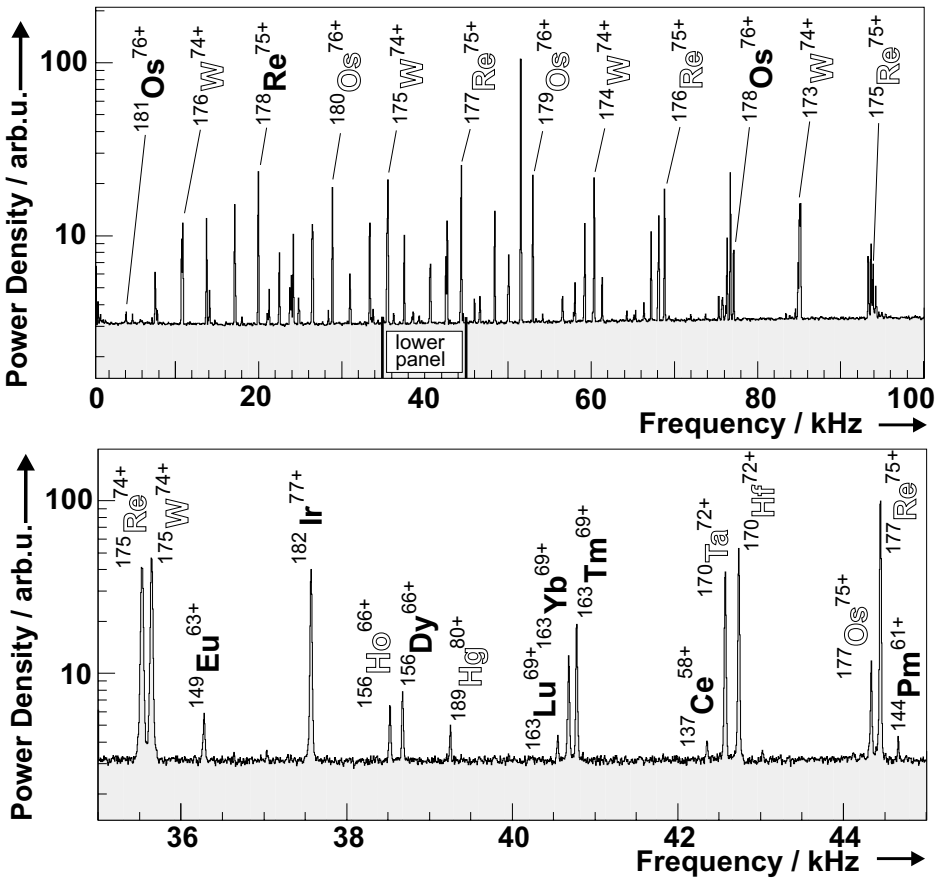

Figure 6: Upper panel: Low-resolution (100-kHz bandwidth) Schottky spectrum of stored and cooled fragments measured for 160 s at a $B\rho$ setting of 7.1 Tm. The frequency scale denotes the difference between the 16^{th} harmonic of the revolution frequency and an admixed external frequency of 30.700 MHz. Lower panel: High-resolution (10-kHz bandwidth) Schottky-spectrum. Most of the frequency lines split up into isobaric doublets or triplets characterized by the same ionic charge. The peaks of ions with known masses used for calibration are indicated by bold letters; nuclei with previously unknown masses are indicated by outlined letters.

(I = 250 mA) were set to optimize the transmission and the cooling of fragments with mass-to-charge ratios of about 2.35. The spectrum contains about 90 different nuclear species in bare, hydrogen-like, or helium-like charge states as presented in Fig. 4. However, isobaric triplets characterized by equal A and q, cannot be resolved in such a 100-kHz broadband spectrum. The necessary m/q resolving power is obtained by the high frequency resolution of the 10-kHz spectra. Only these spectra were used for the mass determination. As an example, such a high-resolution spectrum is displayed in the lower part of Fig 6. The spectrum is an average of 1000 single FFT-spectra and recorded under the same conditions as the 100-kHz spectrum in Fig. 6. The isobars with the same ionic charge states are clearly resolved [26].

The identification of the peaks in the Schottky spectra has been performed by a computer assisted peak pattern comparison [25]. In this procedure the known atomic masses of nuclides from Refs. [6, 7] were corrected for the missing electrons and for the electron binding energies [34, 35, 36]. Based on the input values of the cooler

voltage, the momentum compaction factor α_p, and the local oscillator frequency a 100-kHz frequency spectrum was generated with those masses which were expected from Monte-Carlo simulation to enter into the ESR. After the peak pattern of the 100-kHz spectra was identified, high-resolution spectra with a bandwidth of 10-kHz were recorded and the identification was verified. Depending on the charge of the ions often less than 10 particles were necessary to detect the revolution frequency of an isotope. This sensitivity requires about 1000 averages for a 10-kHz FFT spectrum, where each average took 160 ms. Including the time for electron cooling in addition we were able to access nuclei with effective half-lives longer than 10 s. This holds for nuclear decay modes which are independent of the number of bound electrons.

3 The mass evaluation

In total about 12000 frequency peaks in about 1100 spectra with a bandwidth of 10 kHz were investigated. Different methods of analyzing the Schottky frequency spectra [24, 25] have been employed to extract and to check the mass values. In a first step of data analysis the mass values were determined by using the known masses as a reference in a linear regression [25]. The nonlinearity of α_p as a function of frequency required a calibration for each 10-kHz spectrum. Afterwards the mass value obtained for each isotope was corrected for their charge states and the results for each isotope were averaged. The total errors range from 50 keV, and for very few cases, up to several 100 keV and are in good agreement with the results obtained by a general correlation analysis which will be discussed in detail in the following. A maximum likelihood method [37] has been applied in the evaluation of the masses and their errors. This was performed under the following assumptions:

1. The dependence of the mass-to-charge ratio on the frequency is described by a first order polynomial.

2. 113 reference masses [8] were used for calibration. These nuclei have no isomeric states according to Ref. [8]. This requirement was also applied for the nuclei decaying by emission of α-particles [6].

3.1 The basic equations

In the following the index j represents a specific Schottky spectrum, which consists of frequency peaks. Each peak denoted by μ corresponds to an isotope in a specific charge state. The mass-to-charge ratio deviates randomly from the linear calibration ansatz. The difference is a statistical variable with a mean value equal to zero and a standard deviation Δ_j^μ.

$$\frac{M_j^\mu}{q_j^\mu} - a_j^0 - a_j^1 x_j^\mu = l_j^\mu \pm \Delta_j^\mu. \tag{4}$$

M_j^μ and q_j^μ represent the mass and charge state of the ion connected with the frequency peak x_j^μ. In a good approximation the statistical variable l_j^μ has a Gaussian distribution with a width proportional to standard deviation $\sigma_{x_j^\mu}$ of the frequency peak

$$\Delta_j^\mu = s\sigma_{x_j^\mu}. \tag{5}$$

The scaling factor s is unknown and can be deduced from the maximum likelihood condition (14). For known masses quoted with an accuracy [7] $\Delta\tilde{M}_\gamma$ we assume:

$$M_\gamma^b - \tilde{M}_\gamma^b = l_\gamma \pm \Delta\tilde{M}_\gamma, \tag{6}$$

where $\tilde{M}_\gamma^b$ denotes a known mass from [7] of a bare nuclide and M_γ^b is the mass of the same isotope determined by SMS. l_γ is the statistical variable with a mean value equal to zero forming a Gaussian distribution. The masses and the Q-values in the α-decay chain are related by:

$$M_\alpha^m - M_\alpha^d - m_\alpha - \tilde{Q}_\alpha^b = l_\alpha \pm \Delta\tilde{Q}_\alpha, \tag{7}$$

where M_α^m, M_α^d are two bare nuclides (mother and daughter) characterized by the energy $\tilde{Q}_\alpha^b$ taking into account the differences of bare and neutral atoms involved, determined with an accuracy of $\Delta\tilde{Q}_\alpha$. m_α is the mass of the α particle and l_α is again the statistical variable with mean value equals zero and Gaussian distribution. The Gaussian distribution is defined by the expression:

$$f(l,\sigma) = \frac{1}{\sqrt{2\pi}\sigma}\exp\left[-\frac{l^2}{2\sigma^2}\right]. \tag{8}$$

The method of maximum likelihood consists of estimating the set of masses, coefficients of the calibration curve and the scaling factor, which maximize the joint probability density function L. The global likelihood function L can be written as

$$L = L_c \cdot L_{EXP}. \tag{9}$$

The "experimental" part of the likelihood function, denoted by L_{EXP}, is defined as follows:

$$L_{EXP} = \prod_{j,\mu} f(l_j^\mu, \Delta_j^\mu), \tag{10}$$

where j enumerates the spectra and the index μ runs over all peaks within a given spectrum j.

The calibration term L_c of the likelihood function has the form

$$L_c = \prod_\gamma f(l_\gamma, \Delta\tilde{M}_\gamma) \prod_\alpha f(l_\alpha, \Delta\tilde{Q}_\alpha), \tag{11}$$

where γ runs over reference nuclides with known masses and α runs over α-decay chains with measured Q_α values.

The maximum of the global likelihood function L, as a function of the masses M_μ^b, the coefficients of the calibration curve a_j^k and the scaling factor s can be found by solving the equations

$$\frac{\partial \ln L}{\partial a_j^k} = 0 \qquad k = 0,1\,;\;\; j = 1,2,\ldots,N_S, \tag{12}$$

$$\frac{\partial \ln L}{\partial M_\mu^b} = 0 \qquad \mu = 1,2,\ldots,N_n, \tag{13}$$

$$\frac{\partial \ln L}{\partial s} = 0. \tag{14}$$

Here, N_S and N_n denote the number of used spectra and the number of different nuclides, respectively. The index k enumerates the polynomial coefficients.

3.2 Solution of the basic equations

The solution of eq. (12) yields the two unknown polynomial coefficients for every spectrum j:

$$\hat{\mathbf{A}}_j \begin{pmatrix} a_j^0 \\ a_j^1 \end{pmatrix} = \sum_\mu w_j^\mu \frac{M_j^\mu}{q_j^\mu} \begin{pmatrix} 1 \\ x_j^\mu \end{pmatrix}, \tag{15}$$

where

$$w_j^\mu = \frac{1}{\Delta_j^{\mu\,2}} = \frac{1}{s^2 \sigma^2_{x_\mu^j}} \tag{16}$$

and

$$\hat{\mathbf{A}}_j = \begin{pmatrix} \sum_\mu w_j^\mu & \sum_\mu w_j^\mu x_j^\mu \\ \sum_\mu w_j^\mu x_j^\mu & \sum_\mu w_j^\mu \left(x_j^\mu\right)^2 \end{pmatrix}. \tag{17}$$

The sum $\sum_\mu$ in the matrix $\hat{\mathbf{A}}_j$ and on the right-hand side of eq. (15) runs over all peaks in the spectrum denoted by the index j.

The coefficients a_j^0 and a_j^1 can be calculated from the formula

$$\begin{pmatrix} a_j^0 \\ a_j^1 \end{pmatrix} = \hat{\mathbf{A}}_j^{-1} \sum_\mu w_j^\mu \frac{M_j^\mu}{q_j^\mu} \begin{pmatrix} 1 \\ x_j^\mu \end{pmatrix}, \tag{18}$$

where

$$\hat{\mathbf{A}}_j^{-1} = \frac{1}{\det(\hat{\mathbf{A}}_j)} \begin{pmatrix} \sum_\mu w_j^\mu \left(x_j^\mu\right)^2 & -\sum_\mu w_j^\mu x_j^\mu \\ -\sum_\mu w_j^\mu x_j^\mu & \sum_\mu w_j^\mu \end{pmatrix}. \tag{19}$$

The mass of an ion M_j^μ is equal to the mass of the bare nucleus M_μ^b plus the mass of the bound electrons E_j^μ. Thus, we can write

$$M_j^\mu = M_\mu^b + E_j^\mu. \tag{20}$$

The equation (13) for the mass M_μ^b has the form

$$\sum_j w_j^\mu \frac{M_j^\mu}{\left(q_j^\mu\right)^2} - \sum_j w_j^\mu \frac{\hat{f}_j\left(x_j^\mu\right)}{q_j^\mu} - \frac{\partial ln L_c}{\partial M_\mu^b} = 0, \tag{21}$$

where the sum $\sum_j$ runs over all spectra in which the nuclide appears. This implies that we have as many equations (21) as different nuclides.

The value of the function $\hat{f}_j$ at x_j^μ can be written in the form

$$\hat{f}_j\left(x_j^\mu\right) = a_j^0 + a_j^1 x_j^\mu = \left(1, x_j^\mu\right) \begin{pmatrix} a_j^0 \\ a_j^1 \end{pmatrix}. \tag{22}$$

The last expression (22), together with equations (18) and (21) gives us the final set of equations for the mass values

$$\sum_j \frac{M_j^\mu w_j^\mu}{\left(q_j^\mu\right)^2} - \sum_{j,\beta} \frac{w_j^\mu}{q_j^\mu} \left[\left(1, x_j^\mu\right) \hat{\mathbf{A}}_j^{-1} \begin{pmatrix} 1 \\ x_j^\beta \end{pmatrix} \frac{w_j^\beta M_j^\beta}{q_j^\beta} \right] - \frac{\partial ln L_c}{\partial M_\mu^b} = 0. \tag{23}$$

Here, the index j denotes the spectrum in which the nuclide M_μ^j occurs and the index β runs over all nuclides within the spectrum labeled by j. The equation (23) may be written symbolically

$$\mathbf{W}\vec{M}^b = \vec{w}. \tag{24}$$

Here, the symmetric matrix $\mathbf{W}$ has the dimensions $N_n \times N_n$, where N_n denotes the number of nuclides. The elements of the matrix $\mathbf{W}$ have the form:

$$W_{\mu\mu} = \sum_j \frac{w_j^\mu}{\left(q_j^\mu\right)^2}\left[1 - w_j^\mu \left(1, x_j^\mu\right) \hat{\mathbf{A}}_j^{-1} \begin{pmatrix} 1 \\ x_j^\mu \end{pmatrix}\right] + \frac{1}{\left(\Delta\tilde{M}_\mu\right)^2} + \frac{1}{\left(\Delta\tilde{Q}_\alpha^\mu\right)^2}, \tag{25}$$

$$W_{\mu\nu} = -\sum_j \left[\frac{w_j^\mu w_j^\nu}{q_j^\mu q_j^\nu}\left(1, x_j^\mu\right) \hat{\mathbf{A}}_j^{-1} \begin{pmatrix} 1 \\ x_j^\nu \end{pmatrix}\right] - \frac{1}{(\Delta\tilde{Q}_\alpha^\nu)^2}, \qquad \text{for } \mu \neq \nu. \tag{26}$$

$$\tag{27}$$

The vector $\vec{w}$ can be written as

$$w_\mu = \frac{\tilde{M}_\mu^b}{\left(\Delta\tilde{M}_\mu\right)^2} \pm \frac{m_\alpha + \tilde{Q}_\alpha^b}{\left(\Delta\tilde{Q}_\alpha\right)^2} + B_\mu, \tag{28}$$

where the first term is added when the $\tilde{M}_\mu^b$ is mass of a reference nuclide, the second term has a plus sign if the nuclide is a mother nucleus in the α-decay chain and a minus sign if it is a daughter. The last term is

$$B_\mu = \sum_{j,\beta} \frac{w_j^\mu w_j^\beta}{q_j^\mu q_j^\beta}\left(1, x_j^\mu\right) \hat{\mathbf{A}}_j^{-1} \begin{pmatrix} 1 \\ x_j^\beta \end{pmatrix} E_j^\beta - \sum_j \frac{w_j^\mu E_j^\mu}{\left(q_j^\mu\right)^2}. \tag{29}$$

The equation (14) has been used for the determination of the scaling parameter s

$$\frac{1}{N_n} \cdot \sum_{j,\mu} \frac{l_j^{\mu 2}}{{\sigma_{x_j^\mu}}^2} = s^2. \tag{30}$$

The equations (24) and (30) have been solved iteratively and convergence has been reached after 8 steps. The scaling parameter s has been found to be equal to 0.000163 u kHz^{-1}e $^{-1}$.

3.3 Error Estimation

For each nuclide with the index μ and the mass M_μ^b the diagonal elements of the inverse matrix $\mathbf{W}^{-1}$ have been used to determine the statistical error:

$$\left(\sigma_{M_\mu^b}^{stat}\right)^2 = \mathbf{W}^{-1}{}_{\mu\mu}, \tag{31}$$

This error includes the uncertainties from the reference nuclei and from the Q_α-values [6, 7, 8, 38] used for the determination of the mass under investigation as well as the errors in the frequency determination and the number of measurements for each isotope. The result is that the statistical error is approximately 10 keV for nuclei which are linked to numerous reference nuclei whereas up to 100 keV appears for a few unfavorable cases.

The systematic error has been estimated in a separate evaluation. Only those reference nuclides with mass uncertainties of less than 30μu [7] (82 isotopes) were used for calibration in this investigation. The goal was to determine the masses of the reference nuclei characterized by a mass uncertainty of larger than 30μu [7] ($N_k = 31$ isotopes). A comparison of these mass values M^b_γ with their corresponding tabulated values $\tilde{M}^b_\gamma$ [7] led to a systematic error of σ^{syst}=100 μu derived with the following equation:

$$\sum_\gamma \frac{\left(M^b_\gamma - \tilde{M}^b_\gamma\right)^2}{\left(\Delta\tilde{M}^b_\gamma\right)^2 + (\sigma^{syst})^2 + (\sigma^{stat}_\gamma)^2} = N_k, \tag{32}$$

In the analysis of the data it was observed that neighboring frequency peaks with a distance closer than about 90 Hz cause correlated deviations from the mass-to-charge ratio deduced from the calibration curve. Such deviations for all the reference nuclei are plotted in Fig. 7 for their nearest neighboring frequency peaks. The correlation for those peaks with a relative distance of less than 90 Hz is clearly seen, therefore, those peaks have been discarded from our mass analysis. In spite of this selection residual frequency shifts are assumed to be a major reason for the systematic error in our measurement. The frequency shifts are similar to the cyclotron frequency shifts in Penning traps [39]. Due to a high number of ions circulating with close distances next to each other in the ESR, Coulomb interactions may lead to collective coupled motions.
The results of our general maximum likelihood method is in good agreement with other preceding methods of mass evaluation [25, 26] of the same experiment, where different calibration procedures and selection criteria were applied.

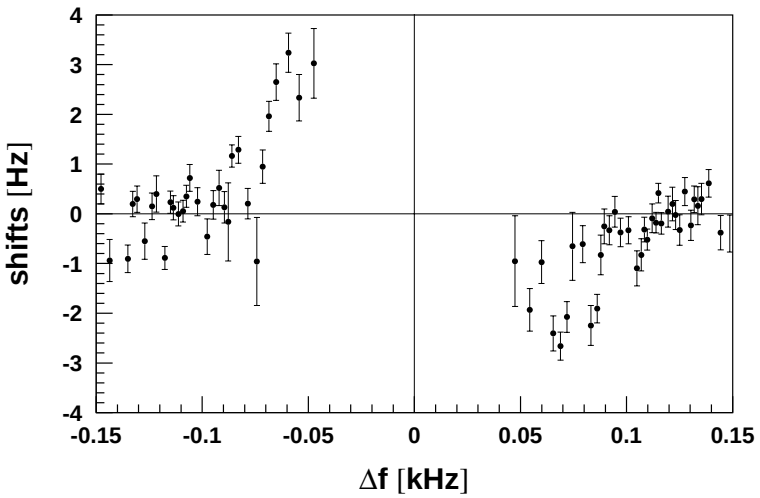

Figure 7: Deviations of the mass-over-charge ratio from the calibration curve versus the distance to the nearest neighboring frequency peak. The distance is assumed positive for a particle on an inner trajectory The closed circles and the error bars represent the mean value and the width for an ensemble of 100 mass-over-charge deviations.

3.4 Table of masses

We present below the table of masses which were directly measured by Schottky mass spectrometry. The table contains only the nuclides for which the masses have been measured for the first time (115 cases) or for nuclides whose mass values were known previously with a precision of worse than 150 keV (6 cases, which are labeled by the index r in the last column of the table). The atomic mass values for nuclides are given in the fifth column in atomic units (u). The error bars for the mass values are shown in the sixth column in μu. The final error presented in Table 1, rounded by the last digit, is the quadratic sum of the statistical and systematic errors. The mass excess values are given with error bars in keV in the seventh and eighth columns, respectively. The number of identified peaks in bare, hydrogen-like, helium-like and lithium-like ions are shown in a separate column. Nuclei which may be contaminated by unresolved isomeric states are marked by an asterisk. For all other nuclei a non-desired mass shift due to isomeric contributions can be excluded by short effective half-lives (less than 10 s) and small excitation energies (less than 100 keV). An elegant way to decide on interference of isomeric state is to use information from α-spectroscopy from the decay chains [40]. This method is applied and the corresponding nuclei are indicated by the index α.

Table 1: Table of masses measured directly at GSI
^{r} - nuclides which masses were known with error bars $\geq$ 150 keV,
* - mass values which may have contaminations by isomeric states,
$^{\alpha}$ - Ground- and Isomeric-States were identified by using information from alpha-spectroscopy (see ref. [40]).

El.	Z	N	A	Exp. mass (u)	Err (μu)	Mass exc. (keV)	Err (keV)	Charge states 0e$^-$	1e$^-$	2e$^-$	3e$^-$	Comm.
La	57	76	133	132.908200	120	-85520	110	1				
Ce	58	76	134	133.908810	130	-84940	120		1			
Nd	60	75	135	134.918200	130	-76200	120			2		
	60	78	138	137.911940	130	-82030	120			1		
Pm	61	77	138	137.919750	140	-74750	130			3		*
Ho	67	89	156	155.929970	110	-65230	100	2	16	3		
Er	68	90	158	157.929780	110	-65410	100	8	13	2		
Tm	69	89	158	157.936920	110	-58760	100			4		
	69	91	160	159.935270	120	-60300	110		4			r
Yb	70	90	160	159.937560	120	-58160	110			4		
	70	91	161	160.937880	110	-57860	100		6	5		
	70	92	162	161.935790	110	-59810	100		5	16		
	70	94	164	163.934310	100	-61190	100	14	29	2		
Lu	71	91	162	161.943390	140	-52730	130			2		*
	71	92	163	162.941270	110	-54710	100		7	7		
	71	93	164	163.941250	110	-54730	100		10	8		
	71	95	166	165.939870	110	-56010	100		16	1		r
Hf	72	92	164	163.944380	110	-51810	100			1	3	
	72	93	165	164.944640	140	-51570	130			3		
	72	94	166	165.942140	110	-53900	100			12	1	
	72	95	167	166.942510	110	-53550	100		9			
	72	96	168	167.940440	100	-55480	100	28	40	17		
	72	98	170	169.939600	100	-56260	100	49	30			
	72	99	171	170.940440	100	-55480	100	54	9	1		
Ta	73	94	167	166.948130	120	-48320	110			3		
	73	95	168	167.947980	110	-48460	100		13	7		
	73	96	169	168.946040	110	-50260	100		15	20		
	73	97	170	169.946190	100	-50120	100	25	47	7		
	73	98	171	170.944450	100	-51740	100	27	84	12		
	73	100	173	172.943730	100	-52420	100	47	5	3		
	73	102	175	174.943650	120	-52490	110	1	3			
W	74	96	170	169.949290	110	-47240	100		3	7	1	
	74	97	171	170.949350	110	-47180	100		14	20		
	74	98	172	171.947230	110	-49150	100	7	28	5		
	74	99	173	172.947660	100	-48750	100	3	64			
	74	100	174	173.946060	100	-50240	100	42	48	11	1	
	74	101	175	174.946710	100	-49640	100	74	37	2		
	74	102	176	175.945580	100	-50690	100	40	13	3		
	74	103	177	176.946580	110	-49760	100	2	4	1		

Re	75	97	172	171.955300	220	-41640	200			1		*
	75	98	173	172.953090	110	-43700	100			20		
	75	99	174	173.953070	100	-43720	100	5	36	27		
	75	100	175	174.951370	100	-45300	100	30	80	28		
	75	101	176	175.951620	110	-45070	100	5	2	9		
	75	102	177	176.950380	100	-46220	100	85	28	7		
	75	103	178	177.951200	110	-45460	100	14	7	2		
Os	76	98	174	173.957120	110	-39940	100			11		
	76	99	175	174.956880	110	-40170	100		9	18		
	76	100	176	175.954850	110	-42060	100			1	1	
	76	101	177	176.954980	100	-41940	100	35	73	15		
	76	102	178	177.953210	100	-43580	100	33	41	6		
	76	103	179	178.953780	100	-43050	100	74	22	5		
	76	104	180	179.952330	100	-44400	100	93	86			
	76	105	181	180.953350	100	-43450	100	52	16	2	1	r
Ir	77	100	177	176.961190	110	-36150	100		1	10	1	
	77	101	178	177.961050	110	-36280	100		5	10		
	77	102	179	178.959090	100	-38110	100	11	50	32	2	
	77	103	180	179.959200	100	-38000	100	2	41	20		
	77	104	181	180.957670	100	-39430	100	38	72	31		
	77	106	183	182.956840	100	-40200	100	85	27	7		
	77	107	184	183.957540	110	-39550	100	1	9			
	77	108	185	184.956660	110	-40370	100	4	7	2		
Pt	78	100	178	177.965700	110	-31950	100			2		
	78	101	179	178.965290	110	-32330	100			16		
	78	102	180	179.963100	110	-34370	100		3	3	5	
	78	103	181	180.963120	100	-34350	100	4	21	34		
	78	104	182	181.961130	100	-36210	100	27	17	1		
	78	105	183	182.961560	100	-35810	90	19	89	29		α
	78	106	184	183.959880	100	-37370	100	81	46	1		
	78	107	185	184.960720	100	-36590	90	126	12	11		r,α
	78	109	187	186.960500	110	-36790	100	16	9	1		
Au	79	102	181	180.969970	110	-27970	100			2		
	79	103	182	181.969580	110	-28340	100		1	11		
	79	104	183	182.967560	100	-30220	100		17	44	3	
	79	105	184	183.967490	100	-30280	100	31	48	26		
	79	106	185	184.965840	100	-31820	90	25	119	7		r,α
	79	108	187	186.964590	100	-32980	90	74	31	6		α
	79	109	188	187.965250	100	-32370	100	7	34	12		
	79	110	189	188.964050	110	-33490	100	23	2			*

Hg	80	104	184	183.971770	110	-26300	100		4	9	1	
	80	105	185	184.971930	100	-26150	90		18	41		α
	80	106	186	185.969340	100	-28560	100	10				
	80	107	187	186.969840	100	-28090	100	1	63	82		*
	80	108	188	187.967540	100	-30240	100	36	37			
	80	109	189	188.968260	100	-29570	100	86	27	12		*
	80	110	190	189.966330	100	-31360	100	122	34	2		
	80	112	192	191.965560	100	-32080	100	90	9	3		
Tl	81	105	186	185.978500	190	-20030	180			5		α
	81	106	187	186.975880	100	-22470	90			18		α
	81	107	188	187.976190	110	-22180	100	6	17	17	3	
	81	108	189	188.973650	110	-24540	100	28	74	50	1	α
	81	109	190	189.973950	100	-24270	100	13	87	12		
	81	110	191	190.971820	100	-26250	90	68	69	32	1	α
	81	111	192	191.972270	100	-25830	100	12	49	14		*
	81	112	193	192.970510	100	-27470	90	79	8	1		α
	81	113	194	193.971340	110	-26700	100	6	11	6		*
	81	114	195	194.969940	100	-28000	100	38	10			
Pb	82	106	188	187.980930	110	-17760	100			1	1	
	82	107	189	188.980810	100	-17880	90			9		α
	82	108	190	189.978060	100	-20440	100		7	12		
	82	109	191	190.978090	110	-20410	100	25	61	56	4	α
	82	110	192	191.975750	100	-22590	100	25	28	7		
	82	111	193	192.976210	100	-22160	100	52	77	23	1	*
	82	112	194	193.974020	100	-24200	100	77	7	1	1	
	82	113	195	194.974690	100	-23580	100	76	40	20		*
	82	114	196	195.972800	100	-25340	100	61	7	2		
	82	115	197	196.973480	110	-24700	100	14	2	4		*
	82	116	198	197.972010	100	-26070	100	30	11			
Bi	83	109	192	191.985290	120	-13700	110		1	3		*
	83	110	193	192.983020	110	-15820	100	1	22	14		
	83	111	194	193.982910	100	-15920	90		58	15		α
	83	112	195	194.980610	100	-18060	90	17	75	17		α
	83	113	196	195.980840	100	-17850	100	84	62	20		*
	83	114	197	196.978890	100	-19660	90	94	35	12		r,α
	83	115	198	197.979230	100	-19350	100	48	25	10		*
Po	84	113	197	196.985690	120	-13330	110		3			*
	84	114	198	197.983400	100	-15470	100	18	2			
	84	115	199	198.983920	100	-14980	100	35	53			*
	84	116	200	199.981830	100	-16930	100	49	2			
	84	117	201	200.982470	100	-16330	100	56	20	1		*
	84	118	202	201.980730	100	-17950	100	28	5	2		

4 Discussion

The mass values presented in Table 1 have been obtained by a data analysis using a least square method. The evaluated mass values are highly correlated in a network which contains repeated measurements for each isotope in different $B\rho$ settings and in many cases in different ionic charge states. The advantage of measuring the same nuclide in different charge states is a unique feature of the present mass experiment. An inherent problem of mass measurements are unresolved isomeric states. One third of the nuclides in Table 1, mainly the odd-odd and the odd-A isotopes of the elements from gold to polonium, have known isomeric states. In principle, we cannot distinguish isomeric states from the ground states if the mass difference is less than the experimental mass resolution. Some criteria can help to estimate the effect of an isomeric state on the mass data given in Table 1. Only states with excitation energies in the range of 100 to 500 keV can considerably change the position of the ground state frequency peak in the spectrum. The isomers with energies higher than 500 keV could in principle be resolved in the spectra. However, we note that none of our nuclei measured was predicted to belong to the latter category. Only isomers with effective half-lives of longer than 10 s exceed the storage and cooling time and can contribute to the frequency peak. Those nuclei, where the above mentioned criteria cannot be applied, might have contributions from isomeric states. These nuclei are marked with an asterisk (*) in Table 1.

Table 1 contains the nuclides for which the mass values have been measured for the

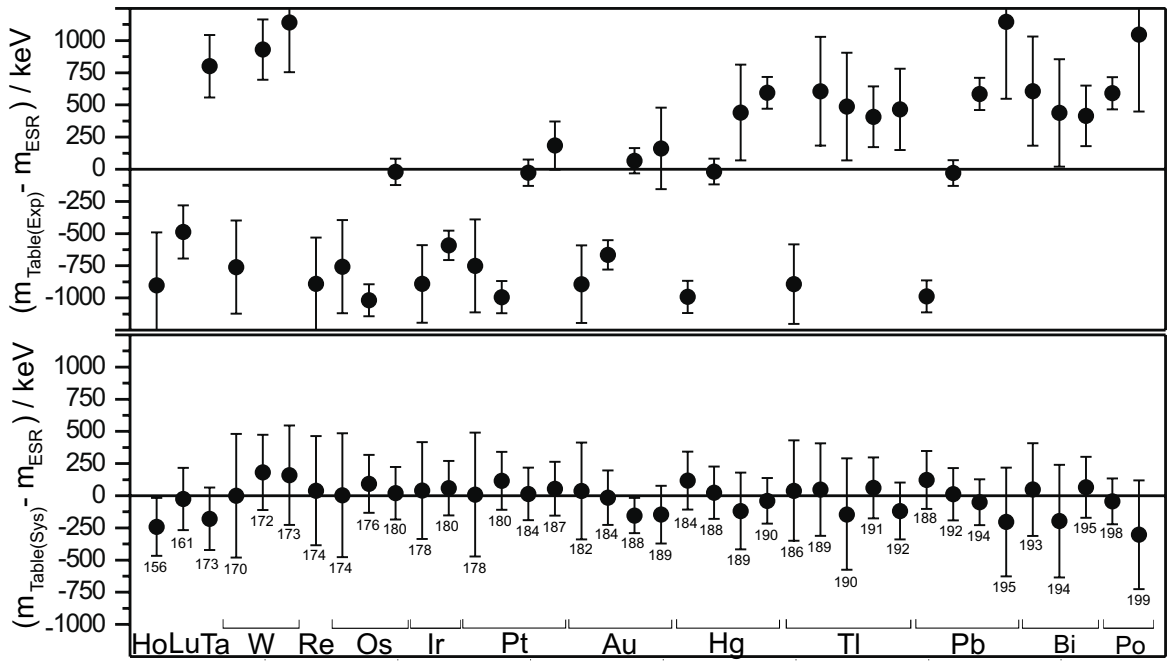

Figure 8: Comparison of previously measured mass data (top) [7][p.479] and mass values recommended by Audi and Wapstra [7] (bottom) with our measured mass values.

first time or were known with poor accuracy. In addition, also mass values for other nuclei are listed which were measured by other methods before but differ drastically from the systematic values given by Audi and Wapstra in Ref. [7]. Evidently, we

did not use those experimental data as reference values in our data analysis and can therefore contribute to decide if the recommended values in Ref. [7] or the published experimental data are more reliable. This comparison is shown in Fig. 8, where the differences are presented between our values and the other experimental and recommended values of Ref. [7]. The result is that our data agree well with the Audi-Wapstra recommendation but strongly disagree with the previous experimental data.
Another check of the reliability of SMS mass data is a comparison (see Fig. 9) with mass values obtained with the Penning trap mass spectrometer ISOLTRAP installed at ISOLDE/CERN [41]. In fig. 9 some of our data are compared to recent ISOLTRAP

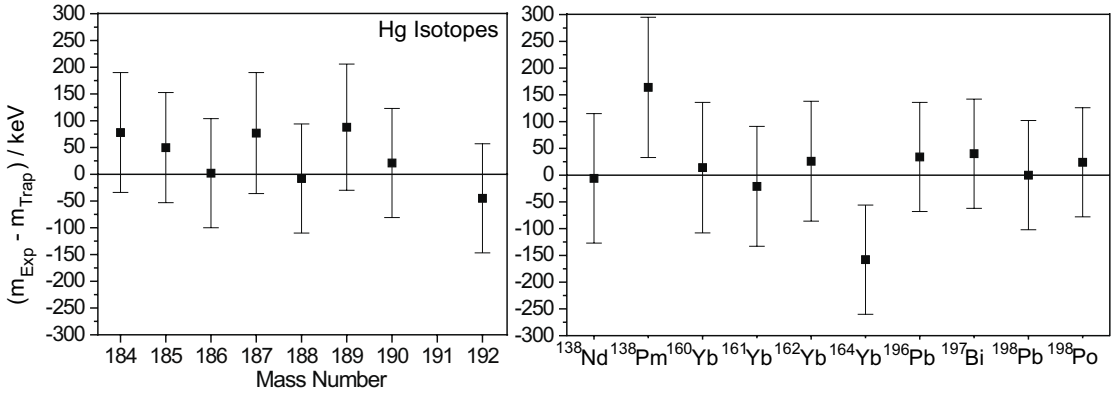

Figure 9: Differences of experimentally determined masses obtained by Schottky Mass Spectrometry and measurements performed by the Penning trap mass spectrometer ISOLTRAP for different isotopes of mercury (left panel) and isotopes of different elements [42] (right panel). In the case of ^{138}Pm most probably a mixture of the ground and the isomeric state was measured. The uncertainty of the ISOLTRAP values of 20–25 keV are included in the error bars.

measurements [42]. The agreement of both experimental data sets is excellent. The mass table of Audi and Wapstra is a comprehensive compilation of experimental data which have been carefully evaluated [7]. From their least-square fit procedures the authors obtain by interpolation and extrapolation also predictions for unknown masses. Therefore, it is interesting to compare our results with these recommended values. A detailed comparison with theoretical models and macroscopic mass formulae will be presented in a forthcoming paper. As a representative comparison with masses listed in the table of Audi and Wapstra [7] we present here only results for the new masses of the elements W, Os, Pt . The differences are shown in Fig. 10 demonstrating that our data are in good agreement with the recommended values of the table. This observation is characteristic for the new mass surface covered in the present experiment, see also Ref. [33].
When all previously unknown masses are included, a calculation of the root mean square deviation (rms) by

$$\sigma_{rms} = \left(\frac{1}{n-1} \sum_{i=1}^{n} (M^i_{exp} - M^i_{table})^2 \right)^{1/2} \tag{33}$$

with experimental M_{exp} and tabulated M_{table} mass values yields an rms deviation of $\sigma_{rms} = 137$ keV, which is quite similar to the errors given in Table 1.

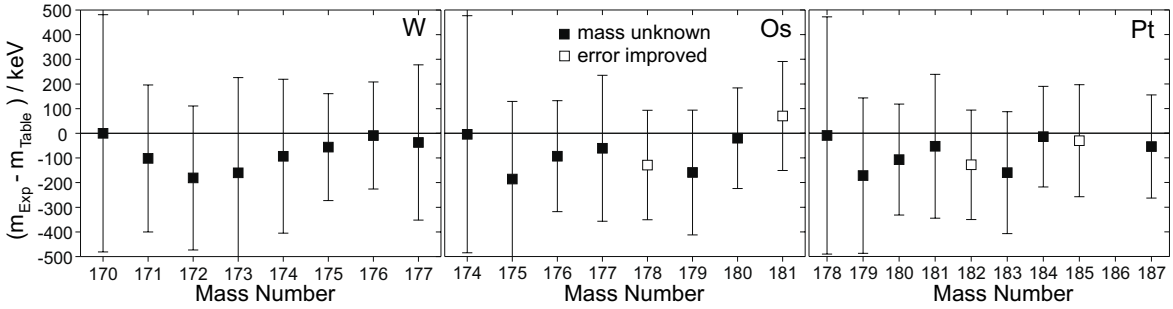

Figure 10: Differences of masses from our experiment obtained by Schottky spectrometry and from the Audi-Wapstra table [7] for the elements tungsten, osmium and platinum. The uncertainties of the mass table are included in the illustrated error bars.

5 Conclusion and Outlook

The combination of the fragment separator FRS and the storage cooler ring ESR is a unique and universal tool to study nuclear properties of relativistic projectile fragments. First comprehensive results on precise mass measurements of exotic nuclei stored and cooled in the ESR at 330–370 MeV/u are presented in this paper. The masses of 105 nuclides in the element range of ($57 \leq Z \leq 84$) have been measured for the first time. The main advantage of SMS is that a large number of different isotopes in a cocktail beam of fragments can be simultaneously stored and cooled in the ESR. The calibration with many reference masses in the same spectrum is advantageous with respect to minimize systematic errors. SMS has a high sensitivity, in the limit the revolution frequency of a single ion can be observed. In the present experiment, the masses of nuclei with half-lives as short as 12 s could be determined which is mainly limited by the electron cooling time.

A number of important improvements for SMS could be achieved recently: The performance of the ESR cooler was considerable improved yielding a much stronger cooling force which led to shorter cooling times and, therefore, gave access to isotopes with slightly shorter half-lives. Furthermore, the better stabilization of the power supplies and the improved field homogeneity of the ESR magnets helped to improve the resolving power by more than a factor 2 in the mass spectra [33]. A new data acquisition system was taken into operation where the digitized signals of the Schottky probes were recorded sequentially with the time stamp of each event. The fast Fourier transformation of these time-correlated data can be performed off-line which gives the advantage that possible drifts during the measurement can be corrected. The new set of data is presently under analysis. An advantage of SMS is that a large mass surface can be mapped in one experiment whereas the ISOLTRAP can be tuned in an experimental cycle on a single isotope only. An ideal combination for mass research in unknown territory can be performed such that a few precisely measured reference masses are determined by a Penning trap system and with SMS a large mass surface is covered to study global structure effects e.g., shell effects and shape changes. A discussion of the features of both methods for mass measurements of exotic nuclei is given in reference [43].

Exotic nuclei with half-lives shorter than the cooling time can be investigated by the

time-of-flight techniques where the ESR is operated in the isochronous mode [44, 45]. In this case, the magnetic fields of the ESR quadrupole and hexapole magnets are set such that the revolution frequency of an ion species becomes independent of its velocity spread, see equation (2). This novel experimental technique has been successfully applied in first measurements with nickel- [45, 33] and chromium fragments ($T_{1/2} < 100$ ms) .
In the future, direct mass measurements will be extended to shorter-lived nuclei using the isochronous method. However, there are also regions on the chart of nuclei where the Schottky mass spectrometry can significantly contribute to improve the knowledge of the mass surface. The better mass resolution as well as the successful development of stochastic cooling in the ESR [47], and using high-sensitive resonant Schottky-probes will considerably enhance the potential of Schottky mass spectrometry of exotic nuclei.

Acknowledgements

Fruitful discussions with G. Audi, H. J. Kluge and A. H. Wapstra are gratefully acknowledged. This work has been financially supported by BMBF under Contract No. 06 GI 4751 and No. 06 LM 363, and the Beschleunigerlaboratorium München. Yu. A. L. and Yu. N. N. would like to thank the GSI and the II. Physikalisches Institut, Universität Giessen for the warm hospitality during their stay in Germany. They also would like to acknowledge the support from the WTZ grant No. RUS-654-96. Z. P. would like to acknowledge for the warm hospitality during his stay at GSI and for the partial support from the Polish Committee for Scientific Research (KBN) grant No. 2P03P11715.

A Reference Nuclides

Table 2: Table of reference nuclei used for determining the masses shown in Table 1. Nuclides which were compared to [7] to determine the systematic error are marked with an ^{s}.

Z	A	Z	A	Z	A	Z	A	Z	A	Z	A
53	125	64	150	68	160^s	72	176	78	188	82	202
54	126	64	151	68	161	73	172^s	78	189	83	202^s
58	136^s	64	152	68	162	73	174^s	78	190	83	203
60	140	65	153	68	163	73	176^s	78	191	83	204
61	141	66	151	69	159^s	73	181	78	192	83	205
61	143	66	152	69	161^s	74	178^s	79	186^s	83	206
61	144	66	153	69	163	74	180	79	190	83	207
61	145	66	154	70	159^s	74	181	79	192	83	208
62	140	66	155	70	163^s	75	179^s	79	194	83	209
62	142	66	156	70	165	75	180^s	79	199	84	194^s
62	145	66	157	70	166	75	181	80	194	84	204
62	146	66	158	70	167	75	189	80	196	84	205^s
63	145	67	155	70	168	76	182	80	198	84	206
63	146	67	157^s	70	173	76	184	81	197^s	84	208
63	147	68	154	71	167^s	76	186	81	199^s	85	201^s
63	148	68	155^s	71	170	77	182^s	81	200	85	203^s
64	147	68	156^s	72	169^s	77	188	81	201	85	204^s
64	148	68	157^s	72	172^s	77	189	81	202	85	205^s
64	149	68	159	72	174	78	186^s	82	200		

B Reference Q_α values

Table 3: Table of Q_α values and their errors (in keV) used additionally for the determination of the masses shown in Table 1.

Z	A	Q_α	ΔQ_α	Z	A	Q_α	ΔQ_α
76	174	4872	10	80	184	5658	15
77	177	5127	10	80	186	5206	15
78	178	5570	3	80	188	4711	3
78	179	5415	10	81	186	5887	149
78	180	5256	10	82	188	6112	3
78	181	5150	5	82	190	5701	4
78	182	4952	5	82	192	5222	5
78	184	4602	3	82	194	4738	20
79	181	5749	3	82	194	6987	3
79	182	5527	5	83	196	6656	3
79	183	5465	3	84	198	6309	2
79	186	4906	15	84	200	5982	2
				84	202	5700	2

References

[1] M. Bender, Doctoral Thesis, University of Frankfurt (1998).

[2] P. Ring, ENAM 98, AIP Conference Proceedings 455 (1998) 22.

[3] W.D. Myers, W. J. Swiatecki, Phys. Rev. C 58 (1998) 3368 .

[4] W.J. Swiatecki. Nucl. Phys. A 574 (1994) 233c.

[5] P.E. Haustein ed. Atom. Data Nucl. Data Tables 39 (1988) 185.

[6] G. Audi and A.H. Wapstra. Nucl. Phys. A 565 (1993) 1.

[7] G. Audi and A.H. Wapstra. Nucl. Phys. A 595 (1995) 409.

[8] G. Audi, O. Bersillon, J. Blachot and A.H. Wapstra, Nucl. Phys. A624, (1997) 1.

[9] A. Gillibert *et al.*, Phys. Lett. B 192, (1987) 39,

[10] J. Wouters *et al.*, Z. Phys. A 331, (1988) 229.

[11] W. Mittig, A. Lepine-Szily, N.A. Orr, Ann. Rev. Nucl. Sci. 47 (1997) 27.

[12] M. Epherre, G. Audi, C. Thibault, *et al.*, Phys. Rev. C 19 (1979) 1504.

[13] I. Bergström, C. Carlberg, R. Schuch, Physica Scripta T 59 (1995).

[14] H.J. Kluge. Proc.ENAM-95 Conf.,Editions Frontiers (1995) 3.

[15] W. Mittig, Nucl. Phys. A 553 (1993) 473c.

[16] G. Bollen, S. Becker, H.J. Kluge *et al.*. Nucl. Instr. Meth. 675 (1996).

[17] B. Franzke, H. Geissel and G. Münzenberg, Mass measurements of stored fragments, GSI-proposal (1987).

[18] M. Steck *et al.*, Phys. Rev. Lett. 77 (1996) 3803.

[19] K. Blasche, B. Franczak, Proc of the third European Part. Acc. Conf., Berlin, 9, eds. H. Henke, H. Homeyer, Ch. Petit-Jean-Genaz. Gif-sur-Yvette: Editions Frontiere (1992).

[20] H. Geissel *et al.*, Nucl. Instr. Meth. B 70 (1992) 286

[21] B. Franzke. Nucl. Instr. Meth. B 24 (1987) 18.

[22] H. Geissel, *et al.*, Phys. Rev. Lett. 68 (1992) 3412.

[23] H. Irnich, H. Geissel, F. Nolden, *et al.*, Phys. Rev. Lett. 75 (1995) 4182.

[24] T. Beha, Doctoral Thesis, University of München (1995).

[25] Th. Kerscher, Doctoral Thesis, University of München (1996).

[26] T. Radon, Th. Kerscher, B. Schlitt *et al.* Phys. Rev. Lett. 78 (1997) 4701.

[27] C. Scheidenberger, Th. Stöhlker, W.E. Meyerhof, *et al.*, Nucl. Instr. and Meth. B 142 (1998) 441.

[28] K. Sümmerer *et al.*, Phys. Rev C 42 (1990) 2546.

[29] N. Iwasa *et al.*, Nucl. Instr. Meth. B 126 (1997) 284.

[30] J. Borer *et al.*, *Proc. IXth Conf. on High Energy Accelerators*, Stanford 1974 (1974) pp. 53.

[31] B. Franzke, Physica Scripta T 59 (1995) 176.

[32] B. Schlitt *et al.*, Hyp. Int. 99 (1996) 117, and Nucl. Phys. A 626 (1997) 315c.

[33] H. Geissel, T. Radon, *et al.*, ENAM 98, AIP Conference Proceedings 455 (1998) 11.

[34] K.N. Huang *et al*, At. Data Nucl. Data Tables 18, 243 (1976).

[35] W.R. Johnson and G. Soff, At. Data Nucl. Data Tables 39 (1988) 265.

[36] D.R. Plante, W.R. Johnson and J. Sapirstein, Phys. Rev. A 49 (1994) 3519.

[37] J.E. Freund, Mathematical Statistics, ed. by Prentice-Hall, Inc., Englewood Cliffs, N.J. (1971).

[38] A. Rytz, Atom. Data Nucl. Data Tables, 47 (1991) 205.

[39] G. Bollen *et al.*, Phys.Rev. C 46 (1992) 46.

[40] Yu. N. Novikov *et al.*, to be submitted to Nucl. Phys. A.

[41] G. Bollen, Physica Scripta T 59 (1995) 165.

[42] S. Schwarz, Doctoral Thesis University of Mainz (1998), unpublished.

[43] H. Geissel, G. Bollen, B. Franzke *et al.*, Nucl. Instr. and Meth. B 126 (1997) 351.

[44] H. Wollnik *et al.*, GSI-Report 86-1 (1986) 372.

[45] M. Hausmann *et al.*, GSI-Report 98-1 (1998) 170.

[46] M. Hausmann *et al.*, Proc. of EPAC conference 1998.

[47] F. Nolden, B. Franzke, A. Schwinn, GSI-Report 98-1 (1998) 171.